Lab on a Chip

Optofluidic Time-stretch Imaging - an Emerging Tool for High-Throughput Imaging Flow Cytometry

Journal:	*Lab on a Chip*
Manuscript ID	LC-CRV-11-2015-001458.R1
Article Type:	Critical Review
Date Submitted by the Author:	31-Mar-2016
Complete List of Authors:	Lau, Andy K. S.; The University of Hong Kong, Department of Electrical and Electronic Engineering Shum, Ho Cheung; University of Hong Kong, Mechanical Engineering Wong, Kenneth K. Y.; The University of Hong Kong, Department of Electrical and Electronic Engineering Tsia, Kevin; The University of Hong Kong, Department of Electrical and Electronic Engineering

Received 00th January 20xx,

Accepted 00th January 20xx

DOI: 10.1039/x0xx00000x

www.rsc.org/

Optofluidic Time-Stretch Imaging – an Emerging Tool for High-Throughput Imaging Flow Cytometry

Andy K. S. Lau[a], Ho Cheung Shum[b], Kenneth K. Y. Wong[a], and Kevin K. Tsia[a]

Optical imaging is arguably the most effective tool to visualize living cells with high spatiotemporal resolution and in a nearly noninvasive manner. Driven by this capability, state-of-the-art cellular assay techniques have increasingly been adopting optical imaging for classifying different cell types/stages, and thus dissecting the respective cellular functions. However, it is still a daunting task to image and characterize cell-to-cell variability within an enormous and heterogeneous population – an unmet need in single-cell analysis, which is now widely advocated in modern biology and clinical diagnostics. The challenge stems from that current optical imaging technologies still lack the practical speed and sensitivity for measuring of thousands to millions cells down to the single-cell precision. Adopting the wisdom in high-speed fiber-optics communication, optical time-stretch imaging has emerged as a completely new optical imaging concept which is now proven for ultrahigh-throughput optofluidic single-cell imaging, at least 1-2 orders-of-magnitude higher (up to ~100,00 cells/sec) compared to the existing imaging flow cytometers. It also uniquely enables quantification of intrinsic biophysical markers of individual cells – a largely unexploited class of single-cell signatures that is known to be correlated with the overwhelmingly investigested biochemical markers. With the aim of reaching a wider spectrum of experts specialized in cellular assay developments and applications, this paper highlights the essential basics of optical time-stretch imaging, followed by reviewing the recent developments and applications of optofluidic time-stretch imaging. We will also discuss the current challenges of this technology, in terms of providing new insights in basic biology and enriching the clinical diagnostic toolsets.

Introduction

To scrutinize the complex cellular physiology and thus to understand pathogenesis of disease, it is always critical, yet challenging, to identify different cell types, cell stages in their lineages down to single-cell precision [1-8]. Influenced by genetic diversity and/or epigenetic variations, cellular properties (from the molecular to biophysical signatures) are now known to be highly heterogeneous, even within the same type of population [1]. Traditional cellular bioassays perform averaged and bulk measurements of the ensembles of cells. They thus do not reflect the cell-to-cell differences and lead to misinterpretation of the true single-cell characteristics. To make it even more challenging, when it is aimed to detect the unknown and rare cell types, e.g. rare cancer cells, aberrant stem cells, and progenitors, it is mandated to involve a sufficiently large sample size, i.e. thousands to millions individual cells.

There is an arsenal of advanced technologies for single-cell measurement and analysis, from single-cell genotype, transcriptomes, to the higher-level phenotypes [4]. However, they all share a common problem: *higher measurement content comes at the expense of lower throughput, or vice versa*. In the other words, the existing technologies always have a limited "*data momentum*" - a figure-of-merit defined as a product of the measured information content ("data mass") and the measurement throughput ("data velocity"). For instance, by adding imaging capability in flow cytometry, current imaging flow cytometers have to scale down the throughput to ~1000 cells/sec from ~100,000 cells/sec achieved by the gold-standard non-imaging flow cytometers [9-11]. In addition, techniques for single-cell gene expression profiling are available in order to probe deeper into the molecular signatures. However, they can only have a typical throughput of ~100's cells per measurement [12]. The feasibility of scaling their throughput to thousands cells or more within a manageable cost and time still remains elusive.

There is another unspoken predicament in cellular assays, which arise from the overwhelming use of biochemical markers. While they provide remarkably detailed molecular signatures of the cells, they are not without their problems. Not only they involve costly labelling and laborious specimen preparation work, these assays are often ineffective when there is little prior knowledge about the biochemical markers of interest [4]. Exploiting niche markers, which can be coupled with the knowledge of biochemical markers, could have its unique value.

In view of all these challenges, researchers have been searching for disruptive technologies, which can interrogate and characterize individual cells within the enormous and heterogeneous populations at a high speed. One key implication of such technology is its unprecedented "data momentum", i.e. a big-data generator. Among all attempts, high-throughput single-cell optical imaging has especially been of immense interest. Optical imaging can provide quantitative visualization of cells with high spatiotemporal resolution, and thus has long been a ubiquitous analytical tool adopted in cell biology and clinical diagnostics. However, the imaging throughput is primarily limited by the imaging strategies (e.g. the speed of the laser scanning technologies used in laser confocal microscopy [13]), the frame rate of the image sensors [14], the image processing complexity and computation power. These limitations hinder large-scale single-cell imaging and thus analysis.

[a] *Department of Electrical and Electronic Engineering, The University of Hong Kong, Pokfulam Road, Pokfulam, Hong Kong.*
[b] *Department of Mechanical Engineering, The University of Hong Kong, Pokfulam Road, Pokfulam, Hong Kong.*

† Footnotes relating to the title and/or authors should appear here.

Electronic Supplementary Information (ESI) available: [details of any supplementary information available should be included here]. See DOI: 10.1039/x0xx00000x

Originally developed for high-speed optical communication [15-16], optical time-stretch is now proven to enable an entirely new concept of optical imaging which achieves ultrafast imaging at a frame rate as high as MHz – orders-of-magnitude higher than any classical imaging systems [17-19]. We note that various ultrafast optical imaging techniques achieve the temporal resolution in the picosecond regime [20-22]. However, they can only operate in a streak-mode/burst-mode. This is in contrast to time-stretch imaging, which enables continuous real-time operation at the frame time resolution of sub-μs [17] or even sub-ns [23] (Fig. 1) – uniquely making itself a big-data imager.

Apart from its utility for ultrahigh-speed optical coherence tomography for in-vivo tissue imaging [18,24-25], it has also been shown that the imaging strategy of this technology is suitable for imaging single cells in microfluidic flow [17,26-30]. Moreover, it provides image-derived quantitative information related to the single-cell biophysical phenotypes (namely morphology, mechanical properties, and intrinsic optical properties) at a high throughput, ~100,000 cells/sec – valuable yet underexploited parameters complementing the standard single-cell analysis based on biochemical markers. As a result, combined with microfluidic technologies, optical time-stretch represents an appealing tool for single-cell imaging flow cytometry operated with big data momentum.

This paper aims to introduce this new imaging tool to a wide range of researchers specialized in the field of microfluidic-based cellular assays. We will first review the recent advances in imaging flow cytometry and compare them with optical time-stretch imaging. We will then highlight the core concepts of this new imaging technique, followed by reviewing the recent developments of different time-stretch imaging modalities for flow cytometry. We will also discuss its current technological challenges and the outlook in the context of single-cell analysis.

Techniques for High-Throughput Imaging Flow Cytometry

Flow cytometry has long been the gold standard for multiparametric cellular assay adopted in clinical diagnostic and basic research. Scaling the number of measurable parameters, which gives higher dimensional data analysis and thus higher-confidence statistical results, has been one of the main trends in the advanced development of flow cytometers, e.g. the state-of-the-art 18-color flow cytometer [31]. On the other hand, accessing the spatial information of the cells (i.e. size, shape and texture) by imaging can also provide morphological analysis, which is not possible with standard flow cytometers [9,11].

Different imaging approaches have also been incorporated with microfluidic flow cytometry. One of the most common methods, motivated by its compact device size, is parallelization of multiple channels [32-34]. Multiple channels are imaged simultaneously within the large field-of-view (FOV) by the image sensor. Therefore, the throughput of this approach can be increased and is proportional to the number of channels. Massively parallelized imaging up to 384 channels in a single chip has been demonstrated [33]. However, large FOV imaging typically requires imaging lens with lower numerical aperture (NA), i.e. compromising the spatial resolution. Apart from relying on the computationally intensive methods for retrieving high-resolution image in large FOV [35-36], efforts have been primarily focusing on imaging single channel with higher flow speed for achieving high-throughput and high-resolution imaging flow cytometry. Specialized imaging techniques based on coded excitation/detection, fluorescence images of the fast flowing cells can be retrieved [37-38]. For instance, a pseudo-random excitation pulse sequence is illuminated on the flowing cells. The resulting motion-blurred cell image is then computationally de-blurred and reconstructed to produce a blur-free image [38]. Another approach is to employ a two-dimensional (2D) light "sheet" illumination [39-43] perpendicular to the flow direction. In this way, three-dimensional (3D) images of the fast flowing cells can be captured at high spatial resolution. Limited by the camera speed, light-sheet-imaging flow cytometry can achieve moderate throughput up to ~100 cells/sec. Using a concept of frequency division multiplexing, an advanced imaging modality, called fluorescence imaging using radiofrequency-tagged emission (FIRE), has recently been demonstrated to achieve an imaging throughput up to 50,000 cells/sec in a microfluidic channel [44].

While the vast majority of the techniques focuses on the use of fluorescence labels as the image contrast agents because of their exquisite biochemical specificity, label-free imaging approaches are attracting a growing interest in imaging flow cytometry. For example, enhanced absorption contrast of red blood cells (RBCs) can be obtained by dual-wavelength illumination, which is essentially a form of spectral imaging [45]. Such method provides measurement of the quantitative cell mass and cell volume, which are proportional to the concentration of haemoglobin, quantified by the absorbance – revealing insights to the disease condition/state of these cells without fluorescence labels and their associated side-effects and toxicity. On the other hand, quantitative phase contrast imaging has also emerged for label-free cell-type classification based on quantifying the optical phase shift maps of the single cells [46]. Table 1 summaries the current microfluidic-based approaches for imaging flow cytometry mentioned above.

Current imaging flow cytometry techniques prevalently rely on the CCD/CMOS imager technology. However, these traditional camera technologies suffer from the fundamental trade-off between sensitivity and speed – during a short integration time fewer photons are collected leading to loss of sensitivity. This explains the challenge of achieving a single-cell imaging throughput beyond 1,000's cells/sec in those CCD/CMOS-based imaging modalities. There are also some high-speed CMOS cameras operating at a frame rate up to 100,000's frames/sec and beyond. However, pixel binning, which reduces the pixel resolution, is mandated in order to maintain adequate signal-to-noise ratio. It is not uncommon to have the degradation of resolution from 1024 × 1024 pixels to only 10's × 10's pixels when the frame rate is required to

Table 1: Comparison of current microfluidic-based approaches for imaging flow cytometry

Approach		Throughput (cells/sec)	Images contrast	Information delivered	Ref
Parallelized channels		2,275 – 21,000	Bright-field Fluorescence	Physical Biochemical	32
		>1,000	Fluorescence	Biochemical	33
		Up to 1,000,000	Bright-field	Physical	34
Single channel	Coded excitation/ detection	1,000	Fluorescence Backscattering	Biochemical	37
		5,000	Fluorescence	Biochemical	38
	Light-sheet illumination	85	Fluorescence	Biochemical	39
		35	Fluorescence	Biochemical	40
		80	Fluorescence	Biochemical	41-42
		40	Fluorescence	Biochemical	43
	FIRE	50,000	Fluorescence	Biochemical	44
	Dual wavelength measurement	17	Absorption	Quantitative biophysical	45
	Focus-stack	160	Quantitative phase Bright-field	Quantitative biophysical	46

increase from ~1000 frames per second (fps) to ~100,000 fps. Together with the fact that these CMOS cameras often require strong and intense illumination, they are typically not commonly used for high-speed imaging flow cytometry applications. In addition, they often require cooling to reduce thermal noise at the expense of adding system complexity and the cooling cost. Optical time stretch imaging offers a unique solution for achieving high frame rate without sacrificing the sensitivity. Its working principles will be explained in the next section, particularly in the context of microfluidic flow imaging. Detailed description of the system design criteria can be referred to ref. [17,26-30].

Primer of Optical Time-stretch Imaging

Key concepts

The core concept of optical time-stretch imaging lies on ultrafast retrieval of the image information, which is optically encoded in the ultrafast broadband laser pulses. More precisely, it involves two mapping steps (Fig. 2): space-wavelength mapping (spectral encoding) and wavelength-time mapping (time-stretch, or also called dispersive Fourier transformation [47-51]). These two steps are in principle interchangeable. Spectral encoding involves the use of an optical spatial disperser, e.g. diffraction grating or prism [19,26-30,52], to generate a one-dimensional (1D) spectral shower for illumination. As different spatial coordinates are illuminated with different spectral components, one-to-one space-wavelength mapping is achieved. The total spectral bandwidth of the pulse determines the imaging FOV. Therefore, the spatial information of the illuminated specimens (i.e. the cells) is encoded in the spectrum of a broadband pulse. Under a double-pass configuration [29-30,52] (Fig. 2(a)), the transmitted, image-encoded spectral shower is then recombined by the same spatial disperser. Note that 2D spectral shower is also feasible [17], and could be particularly relevant to structured illumination applications [53].

Another step is the wavelength-time mapping, in which a broadband optical pulse is temporally stretched by chromatic (temporal) dispersion, or more precisely group-velocity dispersion (GVD) in a dispersive medium, e.g. a long optical fiber (> few to tens of kilometres). It is essentially a manifestation of the concept called space-time duality - the analogy between Fraunhofer (far-field) diffraction and temporal dispersion [54]. Under the condition of sufficiently large GVD (analogous to the far-field diffraction regime in space), the intensity envelope of the stretched temporal waveform is proportional to the input frequency spectrum [47]. It means that the output temporal waveform essentially forms a Fourier-transform pair with the input pulse. As a consequence, any information stamped in the spectrum of the pulse is converted into the temporal serial data.

It is this serial-time operation empowering continuous broadband single-shot spectral acquisition in real time, simply using a single-pixel photodetector and a high-speed electronic digitizer. The spectral acquisition rate, i.e. the frame rate, is governed by the repetition rate of the pulsed laser (typically ~10's MHz). More importantly, optical amplification can be implemented in-line with this time-stretch process to overcome the fundamental trade-off between optical loss and GVD, hence circumventing the trade-off between sensitivity and speed [17,26-30].

In the case of imaging single cells in microfluidic flow, time-stretch imaging mostly operates in a line scan mode, i.e. the 1D spectral shower illumination is static and interrogates the flowing cells along the orthogonal direction. The line scan rate is thus governed by the repetition rate of the pulsed laser source. The 2D time-stretch image can be reconstructed by combining all the 1D line scans digitally.

Enabling components for optofluidic time-stretch imaging

Light sources

Ultrafast pulsed laser is the key prerequisite for time-stretch imaging. To ensure practical operation, the pulsed laser should exhibit wide optical bandwidth (>10 nm), high-repetition rate

(>10 MHz) and most importantly high pulse-to-pulse stability. While femtosecond or picosecond mode-locked lasers based on the bulk crystals can be employed (e.g. Ti:Sapphire laser), the ultrashort laser pulse (sub-100 fs) is however very susceptible to the disturbance in the ambient environment, not to mention its costly and bulky system. As far as system footprint concern, fiber pulsed laser is more favorable, such as fiber mode-locked lasers, and fiber supercontinuum (SC) sources. Harnessing the complex nonlinear optical effects, SC source has an obvious advantage of its ultrabroadband spectrum (>100 nm). Nevertheless, it is not uncommon to show severe shot-to-shot spectral fluctuation, which directly degrades the time-stretch imaging quality [52]. Such SC instability can be moderately improved by a weak triggering/seeding mechanism [55-58]. Mode-locked fiber lasers, which rely on minimal nonlinear optical effects, perhaps are the most robust light sources for time-stretch imaging by offering the best combination of temporal stability and broadband operation [59-62]. For example, two recently developed fiber lasers, called all-normal-dispersion (ANDi) laser [59] and breathing laser as inertia-free swept source (BLISS) [60,62], provide superior shot-to-shot stability (~1% intensity fluctuation at the single-shot repetition rate up to 26 MHz) and a wide bandwidth up to ~60 nm centered at the wavelength of 1060 nm.

Wavelength-time mapping modules

To ensure high spatial resolution in time-stretch imaging, not only should we rely on high-NA imaging objective lens (i.e. achieving diffraction-limited resolution as in classical optical microscopy), but also highly dispersive element (i.e. high GVD). Different types of dispersive elements, primarily in the optical fiber format, have been adopted for time-stretch imaging, e.g. single-mode fibers (SMFs) [15-19,24-30,47-52,59-60,62], few-mode fibers (FMFs) [63], multi-mode fibers (MMFs) [64] and chirped fiber Bragg gratings (CFBGs) [51,65]. Specifically, SMF, and its dispersion-engineered variants (e.g. dispersion-compensation fiber (DCF) [66]), have been the most viable choice because of its wide availability for many applications, particularly fiber-optic communication. Also, they can achieve high GVD (up to 100 ps/nm-km) and low optical loss (<0.5 dB/km) – favourable for high-resolution time-stretch imaging [48].

However, the majority of prior work on time-stretch imaging has been restricted in the near-infrared (NIR) window of 1550 nm – outside the more favorable spectral window for high-resolution in-vitro and in-vivo biological imaging, i.e. shorter NIR or even visible light (1000 nm and below). This is the wavelength regime in which low water absorption and higher diffraction-limited resolution can be attained. One practical advantage of operating time-stretch imaging at shorter wavelengths is its minimal photothermal effect on the aqueous fluid. As water absorption at 1550 nm (absorption coefficient ~10 cm^{-1}) is considerably higher than that at 1 μm (absorption coefficient ~0.01 cm^{-1}) [67], the absorbed optical power at 1550 nm in the microfluidic channel (with a typical dimension of 100 – 200 μm) can be high enough to induce local heating (e.g. >10 ^{o}C for an optical power of >10 mW [68]). It could eventually disturb the variability of optofluidic bioassays [69]. To this end, efforts have been put to shift the time-stretch operation to shorter NIR. Fortunately, off-the-shelf SMFs for short wavelengths are accessible for time-stretch imaging in the windows of 800 nm [70-72] and 1060 nm [29-30,52,59-60,62-63]. It should be cautioned that these short-wavelength SMFs, despite of their higher GVD (~100 ps/nm-km), are generally more lossy than those telecommunication SMFs. It is fundamentally because of the Rayleigh scattering loss that scales with $1/\lambda^4$.

As high GVD inevitably introduces more optical loss in fiber [48], optical amplification almost cannot be omitted in the time-stretch imaging systems. Not only can it compensate the dispersive loss, but also optical net gain is possible – enhancing the sensitivity without sacrificing the imaging speed. We note that optical amplification is particularly crucial for high-speed imaging (photodetection) as the captured signal is easily buried below the thermal noise floor, which scales with the detection bandwidth [47]. Leveraging the established repertoire of optical amplifiers originally designed for telecommunication applications, time-stretch imaging enjoys a wide range of optical amplifiers which can be used for time-stretch imaging in the 1000-nm and 1550-nm wavelength regimes, including semiconductor optical amplifier, rare-earth-doped fiber amplifier, and nonlinear optical amplifiers [73-74].

Ultrafast microfluidic flow

Traditionally, high flow speed, and thus high-throughput operation in the gold-standard flow cytometers is achieved by incorporating sheath flow in the fluidic channel. In this way, the cells can be hydrodynamically focused and aligned in a single profile along the flow direction [10]. While this classical technique can be readily applicable to the microfluidic platforms, sheathless flow configurations have been demonstrated to offer a compact, low-cost, and highly scalable solution for high-throughput microfluidic-based flow cytometry [34,75]. Specifically, inertial flow mechanism, which is not negligible when the flow rate in microchannels is high, has recently emerged as an intriguing tool to manipulate high-speed microparticle and fluid flow in the microscale system in a highly controllable manner, such as particle ordering, separation, and mixing [76-77]. Indeed, most of the existing demonstrations of optofluidic time-stretch imaging are based on the inertial-flow microfluidic platforms [27,29-30,59,70].

As simple as in a straight microchannel (square or rectangular cross-section) under pressure-driven flow, inertial focusing of particles/cells can be achieved as a result of the balance between the two lift forces – a wall effect lift and a shear gradient lift – that determines the cross-sectional equilibrium position of the particles [78]. This simple geometry design particularly favors high-throughput sheath-less flow cytometry based on parallelized focusing [34,79-80].

Channel geometry can also be manipulated to engineer and enhance the inertial flow focusing effect. One notable design is to introduce channel curvature, e.g. spiral-shaped channels [81-88] and serpentine channels [27,29-30,89-91]. Curving channel is known to induce a secondary flow (vortices) in the channel cross-section, called Dean flow [78,90]. The

strength of this effect depends on the main downstream flow characteristics (characterized by the Reynolds number), the radius of channel curvature and the cross-sectional dimension of the channel. Channel curvature plays an important role in controlling the inertial focusing equilibrium positions by balancing the inertial lift force and the drag force proportional to the Dean flow velocity [90]. Compared to straight channels, curving channels also allow shorter focusing distance, which reduces fluidic resistance and thus affects the upper bound of main flow rate (Fig. 3(a)) [90]. This microfluidic configuration has been found essential for robust optofluidic time-stretch imaging of cancer and blood cells at the record high microfluidic flow speed, as high as ~10 m/s [27,29] (Fig. 3(b)).

As far as single-cell/single-particle imaging concern, it is always desirable to align the cells to a single focal plane (along the optical axis) – minimizing out-of-focus imaging. To this end, three-dimensional (3D) sheathless inertial focusing based on a longitudinally corrugated straight channel has recently been demonstrated [92] (Fig. 3(c)). Such geometry of periodic constriction induces a secondary flow that allows cells/particles to migrate to a single focal plane. This technique has also been employed in optofluidic time-stretch imaging of microbeads at a flow speed up to 1 m/s [70].

Variants of Time-stretch Imaging

Bright-field (BF) illumination mode is the most trivial configuration of time-stretch imaging. The key image contrast in this case arises from light scattering and absorption from the single particles or cells. Note that although fluorescence imaging – the workhorse for cellular assays because of their excellent biochemical specificity – is so far not readily compatible with time-stretch imaging, they are not always ideal, particularly in terms of the complications introduced by the detrimental effects of the fluorescent labels (e.g. cytotoxicity, fluorescence quenching, and photobleaching) and the insufficient knowledge about the biochemical markers of interest in some scenarios. For instance, cell surface markers or transcription factors might not be known for specific fluorescent labelling in order to detect the unknown and rare cell types (e.g. aberrant stem cells, progenitors and rare cancer cells) in a highly heterogeneous population. To this end, BF image contrast often provides another information dimension for single-cell phenotyping, e.g. the biophysical signatures, which are known to be correlated with the biochemical properties, have not been fully exploited.

The high-throughput BF imaging capability brought by time-stretch imaging can find a wide range of applications in which morphological analysis (e.g. size, shape/pattern) of individual particles/cells is essential, but impossible with classical non-imaging cytometry. For example, it can be used for ultrafast real-time monitoring the monodispersity of the large population of droplet emulsion - a useful tool for high throughput digital droplet-based bioassay [93]. These microdroplets are typically generated at a rate of >kHz. Even state-of-the-art high-speed CMOS cameras are not capable of capturing such fast events with high-resolution (Fig. 3(d)). Also, BF time-stretch imaging can be well suited for image-based single-cell analysis of apoptosis, e.g. the morphological response to drugs, at an unprecedentedly high throughput. BF time-stretch imaging has recently been demonstrated for rare breast cancer cell (MCF7 cell line) screening in blood (Fig. 3(e)). High detection accuracy as well as specificity is achieved by using treated metal microbeads (~1 μm in diameter) as the cell surface marker, which is specific to MCF7 cells (by targeting EpCAM, a surface molecule existing on MCF7) and at the same time provides significant BF contrast (by the light scattering from the metal microbeads) [27]. It showed a false positive rate of approximately 10^{-6}, two orders of magnitude better than non-imaging flow cytometry [27].

Harnessing the BF contrast, time-stretch could find niche in general study of intracellular interaction and drug delivery with nanoparticles, many of which have been reported to show strong light absorption and scattering. Notable example is that BF image contrast is proven to be even more effective than fluorescence contrast to quantify the intracellular localization of carbon nanotubes (CNTs) and thus to shed light on the cellular trafficking of CNTs [94].

Relying on light absorption and scattering as the contrast mechanism, standard BF imaging mode is still inadequate to reveal the detailed morphology of the label-free transparent cells with high-contrast. Different label-free phase-contrast time-stretch imaging modalities have been developed for enhancing the imaging contrast at ultrafast frame rates. One example is differential interference contrast (DIC)/Nomarski time-stretch imaging [26]. This modality employed a Nomarski prism and a pair of diffraction gratings to generate two 1D orthogonally-polarized spectral showers for illumination. By interfering the two spectrally-encoded beams using the identical Nomarski prism, one can enhance the image contrast which gives rise a pseudo-3D appearance of the specimen – similar to the concept of classical DIC microscopy. By imaging the unstained white blood cells flowing in a microfluidic channel at a high speed of ~1 m/s, this technique achieved >10-fold improvement in the time-stretch image contrast (Fig. 4(a)) [27,29].

Time-stretch image contrast can also be enhanced without the use of the interference effect. Adopting the concept of Schlieren photography [95-96], another time-stretch imaging modality, called asymmetric-detection time-stretch optical microscopy (ATOM), has been demonstrated for label-free, high-contrast imaging of the single cells (human whole blood and leukemic monocytes) at ultrahigh microfluidic speed (up to 10 m/sec), and with sub-cellular resolution (~1.2 μm) (Fig. 3(b)) [29]. The enhanced image contrast in ATOM also shows a DIC-like effects. This is a result of the phase-gradient contrast generated through oblique detection or illumination, which can be done by partially blocking the image-encoded beam path by a knife-edge, or tilting the beam before being coupled into a fiber. This has an equivalent effect of asymmetric or oblique detection of the image field.

Furthermore, ATOM can simultaneously obtain multiple phase-gradient contrasts from different orientations without sacrificing the imaging speed. Thanks to the wavelength-time mapping in which all the image information is encoded in the single pulses, this can be readily performed by time-

multiplexing the encoded waveforms (each with different phase-gradient contrast) in a single fiber. An intriguing consequence is that simple algebraic subtraction and summation of any two opposite-contrast images result in the differential phase-gradient contrast and the absorption contrast, respectively (Fig. 4(b)-(c)). This method decouples the phase-gradient information from absorption, resulting in further enhancement of the image contrast.

Perhaps the most valuable aspect of time-stretch imaging is its ability to be coupled with quantitative phase contrast imaging (QPI), which altogether forms a powerful platform for high-throughput label-free quantitative single-cell analysis, beyond morphological phenotypes. By mapping the optical phase shift distribution, QPI is proven for quantitative evaluation of the intrinsic single-cell optical phenotypes at nanometer scale [97-104]. For examples, it can quantify single-cell mechanical properties with high sensitivity, e.g. mass, stiffness and membrane tension. These intrinsic properties have been found valuable for quantitative assessment of cellular and subcellular morphology [100]. They can also be used as label-free biomarkers for rare cell screening [103] and disease diagnosis [104-105]. Despite these potentials, the fact that QPI relies on the digital image sensors for image acquisition constrains it within the common tradeoff between imaging sensitivity and speed, and limits the overall measurement throughput. Time-stretch quantitative phase-contrast imaging could therefore uniquely bring the information-rich QPI to an unprecedentedly high-throughput regime.

Quantitative phase-contrast time-stretch imaging can be implemented by configuring an interferometer (e.g. free-space Michelson interferometer) in the BF time-stretch imaging system. In this way, the spectrally-encoded pulsed beam from the sample arm is interfered with its uncoded replica from the reference arm, and is then time-stretched to form the temporal interferograms. Applying the Goldstein's algorithm, the 2D raw phase profile of each cell can be retrieved from the interferograms [30].

It has been demonstrated that the refractive index map, an effective intrinsic disease biomarkers, of the lung tissue section can be revealed by quantitative phase-contrast time-stretch microscopy, operated at 1 MHz line-scan rate [30]. The same system was also employed to deliver high-resolution QPI of single cells (MIHA and HeLa cell lines [30]) under ultra-high speed microfluidic flow (up to 1 m/s) (Fig. 4(d)-(e)). More importantly, the time-averaged phase fluctuation was measured to be as small as milli-radians – well within the typical tolerance required for the typical quantitative cellular analysis by conventional QPI.

Quantitative single-cell analysis enabled by time-stretch imaging

A unique capability of optofluidic time-stretch imaging is its ultrafast measurement of the single-cell biophysical markers, derived from the quantitative phase profile, as well as the morphology (e.g. cell size, degree of irregularity, or sub-cellular complexity) [106-107]. In contrast to biochemical markers, biophysical markers – namely morphology, mechanical properties, and intrinsic optical properties of the cells – have not been in the mainstay of cellular assays. The biophysical information is also habitually decoupled from its biochemical counterpart. Yet, there is increasing evidence that biophysical markers have intimate link to the molecular signatures of the cell, and thus provide additional dimensions to dissect cellular physiology and pathology [97,103-105,108-110]. For example, changes in cellular mechanical properties (e.g. size cell, mass, stiffness) are now known to indicate cell growth, proliferation and differentiation. They also serve as the hallmarks of cancer [103-105,110]. In particular, dry mass profiling has emerged as a quantitative tool to evaluate how the single-cell size, mass and growth are regulated during the cell cycle, an important issue in developmental biology [102, 111-112]. Particularly, dry mass density of the single cell is now known as a significant label-free biomarker for a wide range of applications, e.g. monitoring the cell cycle [112], cellular drug response [113], tracking phases of hypertrophy in chondrocytes [102]. It can be quantified based on the retrieved image phase profile and the specific refractive increments of the cell [111]. The specific refractive increment for most biomolecules (e.g. proteins, nucleic acid), which constitute the dry mass of the cell, typically falls within a narrow range. This simplifies the dry mass density computation process.

Stiffness or deformability of cells is closely related to cytoskeleton and other sub-cellular organelle organization, and has been used as intrinsic biomarkers for detecting cell-cycle stages [114], cancer malignancy [91,114-115], and tracking stem-cell differentiation into specific lineage [116-117]. Because of its label-free detection, biophysical markers are thus particularly attractive for a quick and cost-effective single-cell analysis – complementing the standard analysis based on biochemical markers.

Another valuable single-cell property that can be quantified by quantitative phase time-stretch imaging is angular light scattering (ALS) profile. It can be computed based on Fourier transform light scattering method with the quantitative phase/amplitude time-stretch images, i.e. numerically propagating the measured complex field image to generate a far-field scattering pattern [118]. ALS is proven to provide rich information about both cellular and subcellular structures and correlation with the cellular biochemical compositions [118-119]. This parameter can be treated as the biophysical "fingerprint" of the cell type and is thus well suited for automated statistical classification (Fig. 5).

Outlooks

To enhance the capability of time-stretch imaging for optofluidic single-cell analysis, multimodality is the obvious trend. Specifically, combining fluorescence detection with time-stretch imaging could make multiple biomarkers of a single cell (from the molecular to phenotypic signatures) simultaneously accessible in a single platform. Recent effort has been put to incorporate multi-color (up to 3 colors) fluorescence (non-imaging) detection with the time-stretch optofluidic microscope for high-throughput multiparametric

microparticle profiling [70]. With the ability to gather a multitude of single-cell parameters at an ultrafast rate, time-stretch imaging system could essentially achieve a data momentum up to the scale that is impossible with any existing flow cytometers (Table 2). Consider a 300 x 300 pixels ATOM image for each single-cell, the aggregate data rate for an imaging throughput of 100,000 cells/sec can be about 10 GBytes/sec. Furthermore, the phase retrieval processing and the subsequent quantitative image analysis are often preferably done in real-time or with minimal latency. This could introduce overwhelming burden to the back-end data processing units. To this end, there is an immediate need for techniques that can accelerate the workflow from acquisition, processing and storage of massive volumes of data in real-time. Parallel digital signal processing based on field-programmable gate array (FPGA) and graphic processing unit (GPU) have been employed for hardware acceleration in various high-speed optical bioimaging modalities [27,120-122]. Advanced approach such as hybrid implementation of FPGA and GPU as the distributed accelerator is also possible for further enhancing the data management efficiency. Data compression is another important element to address the big data issue in optical time-stretch-based imaging. Compressive sensing has been shown effective for compressing time-stretch image data down to a compression ratio of 1% while maintaining the image quality [123-124]. Extending the concept from the digital to the analog domain, optical data compression, harnessing the tailored nonlinear GVD in a dispersive fiber, e.g. CFBG, has also been exploited as a "photonic hardware accelerator" to streamline the ultrawide-bandwidth time-stretch signal, and thus to relieve the stringent requirements on prohibitively high-speed electronic back-end [125-127].

Table 2: Comparison between the existing flow cytometers and time-stretch optofluidic imaging system

	Conventional flow cytometers	**Imaging flow cytometers**	**Time-stretch imaging**
Through-put (cells/s)	~100,000	~5,000	~100,000
Imaging capability?	No	Yes	Yes
Quanti-tative informa-tion	Fluorescence Scattered light	Fluorescence images Bright-field images	Bright-field images, Quantitative phase images Fluorescence signals
Aggregate raw data through-put	<1 Mbyte/s	~10 Mbytes/s	~10 Gbytes/s

We note that time-stretch optofluidic imaging can also be employed in conjunction with, if compatible, other powerful microfluidic analytical tools. Notably, it is anticipated that it could find a wide range of applications based on the droplet-based microfluidic technology [128-132], which is now known as a potent tool for compartmentalization, measurement and isolation of single cells or molecules in the monodisperse microdroplet (in picoliter) at high-throughput. Incorporating time-stretch imaging in microfluidics could thus represent a new generation of high-throughput technology that not only can identify the standard molecular signatures, but also scavenge the underexploited single-cell biophysical parameters in order to facilitate deep profiling of single cells. Initial attempt of label-free cell-type classification based on quantitative phase time-stretch imaging has shown promises toward the arena of high-throughput single-cell deep profiling and thus large-scale classification [133]. The capability of gathering such a high-content data (e.g. morphological, phenotypic and molecular) with high throughput will enable a new paradigm in data-driven understanding of complex biological processes, especially to unveil the unknown heterogeneity between different single cells. Also, it can empower a new generation of clinical research in which cells at different stages of differentiation can be detected and rare aberrant cells during early disease process can be quantified.

Acknowledgements

This work was partially supported by grant from Research Grant Council of the Hong Kong Special Administration Region, China (Project No. 17207715, 17207714, 17205215, HKU 720112E) Innovation and Technology Support Programme (ITS/090/14) and University Development Fund of HKU.

References

1 F. Fritzsch, C. Dusny, O. Frick, and A. Schmid, "Single-cell analysis in biotechnology, systems biology, and biocatalysis," *Annu Rev Chem Biomol Eng.* **3**, 129-155 (2012).
2 R. Zare and S. Kim, "Microfluidic platforms for single-cell analysis," *Annu Rev Biomed Eng* **12**, 187-201 (2010).
3 P. Hoppe, D. Coutu and T. Schroeder, "Single-cell technologies sharpen up mammalian stem cell research," *Nat. Cell Biol.* **16**, 919-927 (2014).
4 K. Galler, K. Bräutigam, C. Große, J. Popp and U. Neugebauer, "Making a big thing of a small cell – recent advances in single cell analysis," *Analyst*, **139**, 1237-1273 (2014).
5 T. Schroeder, "Long-term single-cell imaging of mammalian stem cells," *Nat. Meth.* **8**, S30-S35 (2011).
6 D. Wang, S. Bodovitz, "Single cell analysis: the new frontier in 'omics'," *Trends Biotechnol.* **28**, 281-290 (2010).
7 F. Tang, K. Lao, and M. Surani, "Development and applications of single-cell transcriptome analysis," *Nat. Meth.* **8,** S6-S11 (2011).
8 T. Kalisky, P. Blainey, and S. Quake, "Genomic analysis at the single-cell level," *Annu. Rev. Genetics* **45**, 431-445 (2011).

9 D. Basiji, W. Ortyn, L. Liang, V. Venkatachalam, and P. Morrissey, “Cellular image analysis and imaging by flow cytometry,” *Clin Lab Med.* **27**, 653-670 (2007).

10 H. M. Shapiro, *Practical Flow Cytometry* (Wiley-Liss, 2003).

11 N. Barteneva, E. Fasler-Kan, and I. Vorobjev, “Imaging flow cytometry: coping with heterogeneity in biological systems,” *Journal of Histochemistry & Cytochemistry* **60**(10), 723–733 (2012).

12 A. Wu, N. Neff, T. Kalisky, P. Dalerba, B. Treutlein, M. Rothenberg, F. Mburu, G. Mantalas, S. Sim, M. Clarke, and S. Quake, “Quantitative assessment of single-cell RNA-sequencing methods,” *Nature Methods* **11**, 41-46 (2014).

13 J. B. Pawley (Ed.), *Handbook of biological confocal microscopy*, 3rd ed., Springer (2006).

14 M. Baker, "Faster frames, clearer pictures," *Nat. Met.* **8**, 1005–1009 (2011).

15 A. Bhushan, F. Coppinger, and B. Jalali, “Time-stretched analogue-to-digital conversion,” *Electron. Lett.* **34**(11), 1081-1083 (1998).

16 F. Coppinger, A. Bhushan, and B. Jalali, “Photonic time stretch and its application to analog-to-digital conversion,” *IEEE T. Microw. Theory Tech.* **47**(7), 1309-1314 (1999).

17 K. Goda, K. Tsia, and B. Jalali, “Serial time-encoded amplified imaging for real-time observation of fast dynamic phenomena,” *Nature* **458,** 1145–1149 (2009).

18 K. Goda, D. Solli, and B. Jalali, "Real-time optical reflectometry enabled by amplified dispersive Fourier transformation," *Appl. Phys. Lett.* **93**, 031106 (2008).

19 K. Goda, K. Tsia, and B. Jalali, “Amplified dispersive Fourier-transform imaging for ultrafast displacement sensing and barcode reading,” *Appl. Phys. Lett.* **93**, 131109 (2008).

20 A. Velten, D. Wu, A. Jarabo, B. Masia, C. Barsi, C. Joshi, E. Lawson, M. Bawendi, D. Gutierrez, and R. Raskar, “Femto-photography: capturing and visualizing the propagation of light,” *ACM Trans. Graph.* **32(**4), Article 44 (2013).

21 K. Nakagawa, A. Iwasaki, Y. Oishi, R. Horisaki, A. Tsukamoto, A. Nakamura, K. Hirosawa, H. Liao, T. Ushida, K. Goda, F. Hannari, and I. Sakuma,” Sequentially timed all-optical mapping photography,” *Nature Photonics* **8**, 695–700 (2014).

22 L. Gao, J. Liang, C. Li and L. V. Wang, "Single-shot compressed ultrafast photography at one hundred billion frames per second," *Nature* **516**, 74–77 (2014).

23 F. Xing, H. Chen, C. Lei, Z. Weng, M. Chen, S. Yang, and S. Xie, “Serial wavelength division 1 GHz line-scan microscopic imaging,” *Photon. Res. B* **2**(4), 31 (2014).

24 J. Xu, X. Wei, L. Yu, C. Zhang, J. Xu, K. K. Y. Wong and K. K. Tsia, "Performance of megahertz amplified optical time-stretch optical coherence tomography (AOT-OCT)," *Optics Express* **22**, 22498-22512 (2014).

25 J. Xu, C. Zhang, J. Xu, K. K. Y. Wong, and K. K. Tsia, "Megahertz all-optical swept-source optical coherence tomography based on broadband amplified optical time-stretch," *Opt. Lett.* **39**, 622-625 (2014).

26 A. Fard, A. Mahjoubfar, K. Goda, D. Gossett, D. Di Carlo, and B. Jalali, “Nomarski serial time-encoded amplified microscopy for high-speed contrast-enhanced imaging of transparent media,” *Biomed. Opt. Express* **2,** 3387–3392 (2011).

27 K. Goda, *et al.*, “High-throughput single-microparticle imaging flow analyzer,” *Proc. Natl Acad. Sci. USA* **109,** 11630–11635 (2012).

28 F. Qian, Q. Song, E. K. Tien, S. K. Kalyoncu, and O. Boyraz, “Real-time optical imaging and tracking of micron-sized particles,” *Opt. Commun.* **282,** 4672–4675 (2009).

29 T. T. W. Wong, A. K. S. Lau, K. K. Y. Ho, M. Y. H. Tang, J. D. F. Robles, X. Wei, A. C. S. Chan, A. H. L. Tang, E. Y. Lam, K. K. Y. Wong, G. C. F. Chan, H. C. Shum and K. K. Tsia, “Asymmetric-detection time-stretch optical microscopy (ATOM) for ultrafast high-contrast cellular imaging in flow,” *Sci. Rep.* **4**, 3656 (2014).

30 A. K. S. Lau, T. T. W. Wong, K. K. Y. Ho, M. T. H. Tang, A. C. S. Chan, X. Wei, E. Y. Lam, H. C. Shum, K. K. Y. Wong, and K. K. Tsia, “Interferometric time-stretch microscopy for ultrafast quantitative cellular and tissue imaging at 1 µm,” *J. Biomed. Opt.* **19**(7), 076001 (2014).

31 S. Bendall, G. Nolan, M. Roederer, and P. Chattopadhyay, "A deep profiler's guide to cytometry," *Trends Immunol.* **33**(7), 323-332 (2012).

32 E. Schonbrun, S. Gorthi, and D. Schaak, “Microfabricated multiple field of view imaging flow cytometry,” *Lab Chip* **12**(2), 268-273 (2012).

33 B. McKenna, J. Evans, M. Cheung, and D. Ehrlich, “A parallel microfluidic flow cytometer for high-content screening,” *Nat. Methods* **8**(5), 401-403 (2011).

34 S. Hur, H. Tse, and D. Di Carlo, “Sheathless inertial cell ordering for extreme throughput flow cytometry,” *Lab on a Chip* **10**, 274-280 (2010).

35 G. Zheng, R. Horstmeyer and C. Yang, "Wide-field, high-resolution Fourier ptychographic microscopy;" *Nature Photonics* **7**, 739–745 (2013).

36 A. Greenbaum, Y. Zhang, A. Feizi, P. Chung, W. Luo, S.R. Kandukuri, and A. Ozcan, ”Wide-field computational imaging of pathology slides using lensfree on-chip microscopy,” *Science Translational Medicine (AAAS)* **6**(267), 267 (2014).

37 Y. Han, and Y. Lo, “Imaging cells in flow cytometer using spatial-temporal transformation,” *Scientific Reports* **5**, 13267 (2015).

38 S. Gorthi, D. Schaak, and E. Schonbrun, “Fluorescence imaging of flowing cells using a temporally coded excitation,” *Optics Express* **21**(4), 5164-5170 (2013).

39 B. Collier, S. Awasthi, D. Lieu, and J. Chan, “Non-linear optical flow cytometry using a scanned, Bessel beam light-sheet,” *Scientific Reports* **5**, 10751 (2015).

40 R. Regmi, K. Mohan, and P. Mondal, “Light sheet based imaging flow cytometry on a microfluidic platform,” *Microsc. Res. Tech.* **76**, 1101–1107 (2013).

41 J. L. Wu, and R. K. Y. Chan, “A fast fluorescence imaging flow cytometer for phytoplankton analysis,” *Opt. Express* **21**(20), 23921-23926 (2013).

42 J. L. Wu, J. P. Li, and R. K. Y. Chan, “A light sheet based high throughput 3D-imaging flow cytometer for phytoplankton analysis,” *Opt. Express* **21**(12), 14474-14478 (2013).

43 R. Regmi, K. Mohan, and P. M. Partha, “High resolution light-sheet based high-throughput imaging cytometry system enables visualization of intra-cellular organelles,” *AIP Advances* **4**, 097125 (2014).

44 E. D. Diebold, B. W. Buckley, D. R. Gossett, and B. Jalali, “Digitally synthesized beat frequency multiplexing for sub-millisecond fluorescence microscopy,” *Nature Photonics* **7**, 806-810 (2013).

45 E. Schonbrun, R. Malka, G. Di Caprio, D. Schaak, and J. M. Higgins, “Quantitative absorption cytometry for measuring red blood cell hemoglobin mass and volume,” *Cytometry A* **85**, 332–338 (2014).

46 S. S. Gorthi, and E. Schonbrun, “Phase imaging flow cytometry using a focus-stack collecting microscope,” *Optics Letters* **37**(4), 707-709 (2012).

47 K. Goda, D. R. Solli, K. K. Tsia, and B. Jalali, “Theory of amplified dispersive Fourier transformation,” *Phys. Rev. A* **80,** 043821 (2009).

48 T. Jannson, “Real-time Fourier transformation in dispersive optical fibers,” *Opt. Lett.* **8**, 232–234 (1983).

49 Y. C. Tong, L. Y. Chan, and H. K. Tsang, “Fiber dispersion or pulse spectrum measurement using a sampling oscilloscope,” *Electron. Lett.* **33,** 983–985 (1997).

50 P. V. Kelkar, F. Coppinger, A. S. Bhushan, and B. Jalali, "Time-domain optical sensing," *Electron. Lett.* **35,** 1661–1662 (1999).

51 J. Anaza, L. R. Chen, M. A. Muriel, and P. W. E. Smith, "Experimental demonstration of real-time Fourier transformation using linearly chirped fiber Bragg gratings," *Electron. Lett.* **35**, 2223–2224 (1999).

52 T. T. W. Wong, A. K. S. Lau, K. K. Y. Wong, and K. K. Tsia, "Optical time-stretch confocal microscopy at 1 µm," *Opt. Lett.* **37**, 3330-3332 (2012).

53 A. Chan, A. K. S. Lau, K. K. Y. Wong, E. Lam, K. K. Tsia, "Arbitrary two-dimensional spectrally-encoded pattern generation - a new strategy for high-speed patterned illumination imaging," Optica (in print).

54 W. J. Caputi, "Stretch: A time-transformation technique," *IEEE Trans. Aerosp. Electron. Syst.* **AES-7**, 269–278 (1971).

55 D. R. Solli, C. Ropers, and B. Jalali, "Active control of rogue waves for stimulated supercontinuum generation," *Phys. Rev. Lett.* **101,** 233902 (2008).

56 D. R. Solli, B. Jalali, and C. Ropers, "Seeded supercontinuum generation with optical parametric down-conversion," Phys. Rev. Lett. **105**, 233902 (2010).

57 S. T. Sørensen, C. Larsen, U. Møller, P. M. Moselund, C. L. Thomsen, and O. Bang, "Influence of pump power and modulation instability gain spectrum on seeded supercontinuum and rogue wave generation," *J. Opt. Soc. Am. B* **29**, 2875-2885 (2012).

58 K. K. Y. Cheung, C. Zhang, Y. Zhou, K. K. Y. Wong, and K. K. Tsia, "Manipulating supercontinuum generation by minute continuous wave," *Opt. Lett.* **36**, 160-162 (2011).

59 X. Wei, A. K. S. Lau, T. T. W. Wong, C. Zhang, K. K. Tsia, and K. K. Y. Wong, "Coherent laser source for high frame-rate optical time-stretch microscopy at 1.0 µm," *IEEE J. Sel. Top. in Quant. Electron.* **20**, 1100306 (2014).

60 X. Wei, A. K. S. Lau, Y. Xu, K. K. Tsia, and K. K. Y. Wong, "28 MHz swept source at 1.0 µm for ultrafast quantitative phase imaging," *Biomed. Opt. Express* **6**, 3855-3864 (2015).

61 O. Boyraz, J. Kim, M. N. Islam, F. Coppinger, and B. Jalali, "Broadband, high-brightness 10-Gbit/s supercontinuum source for A/D conversion," in *Conference on Lasers and Electro-Optics* (Institute of Electrical and Electronics Engineers, San Francisco, 2000), pp. 489–490.

62 X. Wei, J. Xu, Y. Xu, L. Yu, J. Xu, B. Li, A. K. S. Lau, X. Wang, C. Zhang, K. K. Tsia, and K. K. Y. Wong, "Breathing laser as an inertia-free swept source for high-quality ultrafast optical bioimaging," *Opt. Lett.* **39**, 6593-6596 (2014).

63 Y. Qiu, J. Xu, K. K. Y. Wong, and K. K. Tsia, "Exploiting few mode-fibers for optical time-stretch confocal microscopy in the short near-infrared window," *Opt. Express* **20**, 24115-24123 (2012).

64 E. D. Diebold, N. K. Hon, Z. Tan, J. Chou, T. Sienicki, C. Wang, and B. Jalali, "Giant tunable optical dispersion using chromo-modal excitation of a multimode waveguide," *Opt. Express* **19**, 23809-23817 (2011).

65 T. J. Ahn, Y. Park, and J. Azaña, "Ultrarapid optical frequency-domain reflectometry based upon dispersion-induced time stretching: principle and applications," *IEEE J. Sel. Top. Quantum Electron.* **18**(1), 148–165 (2012).

66 G. P. Agrawal, *Nonlinear Fiber Optics* (Academic Press, 2012).

67 K. K. Tsia (Ed.), Understanding Biophotonics - Fundamentals, Advances and Applications, Pan Stanford Publishing Pte Ltd. (Oct 2014).

68 R. Xu, H. Xin, and B. Li, "Photothermal formation of vortex flows by 1.55 µm light," *AIP Advances* **3**, 052120 (2013).

69 C. B. Maddox, L. Rasmussen, and E. L. White, "Adapting cell-based assays to the high throughput screening platform: problems encountered and lessons learned," *JALA Charlottesv Va.* **13** 168–173 (2008).

70 M. Ugawa, L. Cheng, T. Nozawa, T. Ideguchi, D. Di Carlo, S. Ota, Y. Ozeki, and K. Goda, "High-throughput optofluidic particle profiling with morphological and chemical specificity," *Opt. Lett.* **40**(20), 4803-4806 (2015).

71 K. Goda, *et al.*, "Hybrid dispersion laser scanner," *Sci. Rep.* **2**, 445 (2012).

72 K. Goda, A. Fard, O. Malik, G. Fu, A. Quach, and B. Jalali, "High-throughput optical coherence tomography at 800 nm," *Optics Express* **20**, 19612 (2012).

73 K. Goda, and B. Jalali, "Dispersive Fourier transformation for fast continuous single-shot measurements," *Nature Photonics* **7**, 102–112 (2013).

74 X. Wei, S. Tan, A. Mussot, A. Kudlinski, K. K. Tsia, and K. K. Y. Wong, "110 nm versatile fiber optical parametric amplifier at 1.0 µm," *Opt. Lett.* **40**, 4090-4093 (2015).

75 D. Di Carlo, "Inertial microfluidics," *Lab Chip* **9**, 3038-3046 (2009).

76 A. J. Mach, and D. Di Carlo, "Continuous scalable blood filtration device using inertial microfluidics," *Biotechnol. Bioeng.* **107**, 302–311 (2010).

77 H. A. Nieuwstadt, R. Seda, D. S. Li, J. B. Fowlkes and J. L. Bull, "Microfluidic particle sorting utilizing inertial lift force," *Biomed. Microdevices* **13**, 97–105 (2011).

78 H. Amini, W. Lee, D. Di Carlo, "Inertial microfluidic physics," *Lab Chip* **14**, 2739–2761 (2014).

79 J. Hansson, J. M. Karlsson, T. Haraldsson, H. Brismar, W. van der Wijngaart and A. Russom, "Inertial microfluidics in parallel channels for high-throughput applications," *Lab Chip* **12**, 4644–4650 (2012).

80 A. T. Ciftlik, M. Ettori and M. A. M. Gijs, "High throughput-per-footprint inertial focusing," *Small* **9**, 2764–2773 (2013).

81 S. S. Kuntaegowdanahalli, A. A. Bhagat, G. Kumar and I. Papautsky, "Inertial microfluidics for continuous particle separation in spiral microchannels," *Lab Chip* **9**, 2973–2980 (2009).

82 A. Russom, A. K. Gupta, S. Nagrath, D. Di Carlo, J. F. Edd and M. Toner, "Differential inertial focusing of particles in curved low-aspect-ratio microchannels," *New J. Phys.* **11**, 075025 (2009).

83 W. C. Lee, A. A. S. Bhagat, S. Huang, K. J. Van Vliet, J. Han and C. T. Lim, "High-throughput cell cycle synchronization using inertial forces in spiral microchannels," *Lab Chip* **11**, 1359–1367 (2011).

84 J. M. Martel and M. Toner, "Inertial focusing dynamics in spiral microchannels," *Phys. Fluids* **24**, 032001 (2012).

85 E. W. Kemna, R. M. Schoeman, F. Wolbers, I. Vermes, D. A. Weitz and A. van den Berg, "High-yield cell ordering and deterministic cell-in-droplet encapsulation using Dean flow in a curved microchannel," *Lab Chip* **12**, 2881-2887 (2012).

86 H. W. Hou, M. E. Warkiani, B. L. Khoo, Z. R. Li, R. A. Soo, D. S.-W. Tan, W.-T. Lim, J. Han, A. A. S. Bhagat and C. T. Lim, "Isolation and retrieval of circulating tumor cells using centrifugal forces," *Sci. Rep.* **3**, 1259 (2013).

87 N. Xiang, H. Yi, K. Chen, D. Sun, D. Jiang, Q. Dai and Z. Ni, "High-throughput inertial particle focusing in a curved microchannels: insights into the flow-rate regulation mechanism and process model," *Biomicrofluidics* **7**, 044116 (2013).

88 G. Guan, L. Wu, A. A. Bhagat, Z. Li, P. C. Y. Chen, S. Chao, C. J. Ong and J. Han, "Spiral microchannel with rectangular and trapezoidal cross-sections for size based particle separation," *Sci. Rep.* **3**, 1475 (2013).

89 D. Di Carlo, D. Irimia, R. G. Tompkins and M. Toner, "Continuous inertial focusing, ordering, and separation of particles in microchannels," *Proc. Natl. Acad. Sci. U. S. A.* **104**, 18892–18897 (2007).

90 D. R. Gossett and D. Di Carlo, "Particle focusing mechanisms in curving confined flows," *Anal. Chem.* **81**, 8459–8465 (2009).

91 D. R. Gossett, H. T. K. Tse, S. A. Lee, Y. Ying, A. G. Lindgren, O. O. Yang, J. Rao, A. T. Clark and D. D. Carlo, "Hydrodynamic stretching of single cells for large population mechanical phenotyping," *Proc. Natl. Acad. Sci. U. S. A.* **109**, 7630–7635 (2012).

92 A. J. Chung, D. R. Gossett, and D. Di Carlo, "Three dimensional, sheathless, and high-throughput microparticle inertial focusing through geometry-induced secondary flows," *Small* **9**, 685-690 (2013).

93 J. F. Edd, D. Di Carlo, K. J. Hunphry, K. Koster, D. Irimia, D. A. Weitz, and M. Toner, "Controlled encapsulation of single-cells into monodisperse picolitre drops," *Lab Chip* **8**, 1262-1264 (2008).

94 I. Marangon, N. Boggetto, C. Menard-Moyon, E. Venturelli, M. L. Beoutis, C. Pechoux, N. Luciani, C. Wilhelm, A. Bianco, F. Gazeau, "Intercellular carbon nanotube translocation assessed by flow cytometry imaging," *Nano Lett.* **12**, 4830–4837 (2012).

95 D. Axelrod, "Zero-cost modification of bright field microscopes for imaging phase gradient on cells: Schlieren optics," *Cell Biophys.* **3**, 167–173 (1981).

96 J. G. Dodd, "Interferometry with Schlieren microscopy," *Appl. Opt.* **16**(16), 470–472 (1977).

97 G. Popescu, *Quantitative Phase Imaging of Cells and Tissues*, McGraw-Hill (2011).

98 B. Bhaduri, C. Edwards, H. Pham, R. Zhou, T. Nguyen, L. Goddard, and G. Popescu, "Diffraction phase microscopy: principles and applications in materials and life sciences," *Adv. Opt. Photon.* **6**, 57-119 (2014).

99 A. B. Parthasarathy, K. K. Chu, T. N. Ford, and J. Mertz, "Quantitative phase imaging using a partitioned detection aperture," *Opt. Lett.* **37**, 4062-4064 (2012).

100 M. Kalashnikov, W. Choi, C. Yu, Y. Sung, R. Dasari, K. Badizadegan, and M.S. Feld, "Assessing light scattering of intracellular organelles in single intact living cells," *Opt. Express* **17**, 19674-19681 (2009).

101 Y. Cotte, F. Toy, P. Jourdain, N. Pavillon, D. Boss, P. Magistretti, P. Marquet and C. Depeursinge, "Marker-free phase nanoscopy," *Nat. Photon.* **7**, 113-117 (2013).

102 K. L. Cooper, S. Oh, Y. Sung, R. R. Dasari, M. W. Kirschner and C. J. Tabin, "Multiple phases of chondrocyte enlargement underlie differences in skeletal proportions," *Nature* **495**, 375-378 (2013).

103 K. Phillips, C. Velasco, J. Li, A. Kolatkar, M. Luttgen, K. Bethel, B. Duggan, P. Kuhn and O. McCarty, "Optical quantification of cellular mass, volume, and density of circulating tumor cells identified in an ovarian cancer patient," *Front Oncol.* **18**, 2-72 (2012).

104 Z. Wang, K. Tangella, A. Balla, and G. Popescu, "Tissue refractive index as marker of disease," *J Biomed Opt* **16**, 116017 (2011).

105 P. Wang, R. Bista, R. Bhargava, R. E. Brand, and Y. Liu, "Spatial-domain low-coherence quantitative phase microscopy for cancer diagnosis," *Opt. Lett.* **35**, 2840-2842 (2010).

106 A. Mahjoubfar, C. Chen, K. R. Niazi, S. Rabizadeh, and B. Jalali, "Label-free high-throughput cell screening in flow," *Biomedical Optics Express* **4**(9), 1618-1625 (2013).

107 C. Chen, A. Mahjoubfar, A. Huang, K. Niazi, S. Rabizadeh, and B. Jalali, "Hyper-dimensional analysis for label-free high-throughput imaging flow cytometry," in *CLEO: 2014*, OSA Technical Digest (online) (Optical Society of America, 2014), paper AW3L.2.

108 H. Ding, Z. Wang, X. Liang, S. A. Boppart, K. Tangella, and G. Popescu, "Measuring the scattering parameters of tissues from quantitative phase imaging of thin slices," *Opt. Lett.* **36**, 2281-2283 (2011).

109 A. Fritsch, M. Hockel, T. Kiessling, K. D. Nnetu, F. Wetzel, M. Zink, and J. A. Käs, "Are biomechanical changes necessary for tumour progression," *Nat. Phys.* **6**, 730-732 (2010).

110 J. Guck, S. Schinkinger, B. Lincoln, F. Wottawah, S. Ebert, M. Romeyke, D. Lenz, H. M. Erickson, R. Ananthakrishnan, D. Mitchell, J. Käs, S. Ulvick, and C. Bilby, "Optical deformability as an inherent cell marker for testing malignant transformation and metastatic competence," *Biophys J* **88**, 3689-3698 (2005).

111 T. A. Zangle and M. A. Teitell, "Live-cell mass profiling: an emerging approach in quantitative biophysics," *Nat. Methods* **11**, 1221-1228 (2014).

112 P. Girshovitz, and N. T. Shaked, "Generalized cell morphological parameters based on interferometric phase microscopy and their application to cell life cycle characterization," *Biomedical Optics Express* **3**(8), 1757-1773 (2012).

113 M. Mir, A. Bergamaschi, B. S. Katzenellenbogen, and G. Popescu, "Highly sensitive quantitative imaging for monitoring single cancer cell growth kinetics and drug response," *PLoS ONE* **9**(2), e89000 (2014).

114 O. Otto, P. Rosendahl, *et al.*, "Real-time deformability cytometry: on-the-fly cell mechanical phenotyping" *Nat. Met.* **12**, 199-202 (2015).

115 H. T. Tse, D. R. Gossett, Y. S. Moon, M. Masaeli, M. Sohsman, Y. Ying, K. Mislick, R. P. Adams, J. Rao, D. Di Carlo, "Quantitative diagnosis of malignant pleural effusions by single-cell mechanophenotyping," *Sci Transl Med.* **5**, 212 (2013).

116 J. D. Pajerowski, K. N. Dahl, F. L. Zhong, P. J. Sammak, and D. E. Discher, "Physical plasticity of the nucleus in stem cell differentiation," *Proc Natl Acad Sci* **104**, 15619-15624 (2007).

117 F. Chowdhury, S. Na, D. Li, Y.-C. Poh, T. S. Tanaka, F. Wang and N. Wang, "Material properties of the cell dictate stress-induced spreading and differentiation in embryonic stem cells," *Nat. Mater.* **9**, 82-8 (2010).

118 H. Ding, E. Berl, Z. Wang, L. J. Millet, M. U. Gillette, J. Liu, M. Boppart, and G. Popescu, "Fourier transform light scattering of biological structure and dynamics," *IEEE J. Sel. Top. Quant. Electron.* **16**, 909-918 (2010).

119 Y. Jo, J. H. Jung, J. W. Lee, D. Shin, H. J. Park, K. T. Nam, J.-H. Park and Y. K. Park, "Angle-resolved light scattering of individual rod-shaped bacteria based on Fourier transform light scattering," *Sci. Rep.* **4**, 5090 (2014).

120 H. Pham, H. Ding, N. Sobh, M. Do, S. Patel, and G. Popescu, "Off-axis quantitative phase imaging processing using CUDA: toward real-time applications," *Biomed. Opt. Express* **2**(7), 1781–1793 (2011).

121 A. E. Desjardins, B. J. Vakoc, M. J. Suter, S.-H. Yun, G. J. Tearney, and B. E. Bouma, "Real-time FPGA processing for high-speed optical frequency domain imaging," *IEEE Trans Med Imaging* **28**(9), 1468–1472(2009).

122 D. Xu, Y. Huang, and J. U. Kang, "GPU-accelerated non-uniform fast Fourier transform-based compressive sensing spectral domain optical coherence tomography," *Opt. Express* **22**, 14871-14884 (2014).

123 B. T. Bosworth, and M. A. Foster, "High-speed ultrawideband photonically enabled compressed sensing of sparse radio frequency signals," *Optics Letters* **38**(22), 4892-4895 (2013).

124 B. T. Bosworth, J. R. Stroud, D. N. Tran, T. D. Tran, S. Chin, and M. A. Foster, "High-speed flow microscopy using compressed sensing with ultrafast laser pulses," *Optics Express* **23**(8), 10521-10532 (2015).

125 M. H. Asghari and B. Jalali, "Experimental demonstration of optical real-time data compression," *Appl. Phys. Lett.* **104**, 111101 (2014).

126 C. L. Chen, A. Mahjoubfar, and B. Jalali, "Optical data compression in time stretch imaging," *PLoS ONE* **10**(4), e0125106 (2015).

127 B. Jalali, J. Chan, and M. H. Asghari, “Time-bandwidth engineering,” *Optica* **1**(1), 23–31 (2014).

128 H. N.Joensson, and H. Andersson Svahn, “Droplet Microfluidics—A Tool for Single-Cell Analysis,” *Angew. Chem. Int. Ed.* **51,** 12176–12192 (2012).

129 E. Brouzes, M. Medkova, N. Savenelli, D. Marran, M. Twardowski, J. B. Hutchison, J. M. Rothberg, D. R. Link, N. Perrimon, M. L. Samuels, “Droplet microfluidic technology for single-cell high-throughput screening,” *Proc. Natl. Acad. Sci.* **106**, 14195 – 14200 (2009).

130 M. T. Guo, A. Rotem, J. A. Heymanab and D. A. Weitz, "Droplet microfluidics for high-throughput biological assays," *Lab Chip* **12**, 2146-2155 (2012).

131 L. Mazutis, J. Gilbert, W L. Ung, D. A Weitz, A. D Griffiths & J. A Heyman, "Single-cell analysis and sorting using droplet-based microfluidics," *Nat. Protocols* **8**, 870–891 (2013).

132 O.J. Miller, A. El Harrak, T. Mangeat, JC. Baret, L. Frenz, B. El Debs, E. Mayot, M.L. Samuels, E.K. Rooney, P. Dieu, M. Galvan, D.R. Link, and A.D. Griffiths, "High-resolution dose–response screening using droplet-based microfluidics," *Proc. Natl. Acad. Sci.* **10** 378-383 (2012).

133 C. L. Chen, A. Mahjoubfar, L. Tai, I. K. Blaby, A. Huang, K. R. Niazi, and B. Jalali, “Deep learning in lable-free cell classification,” *Sci. Rep.* **6**, 21471 (2016).

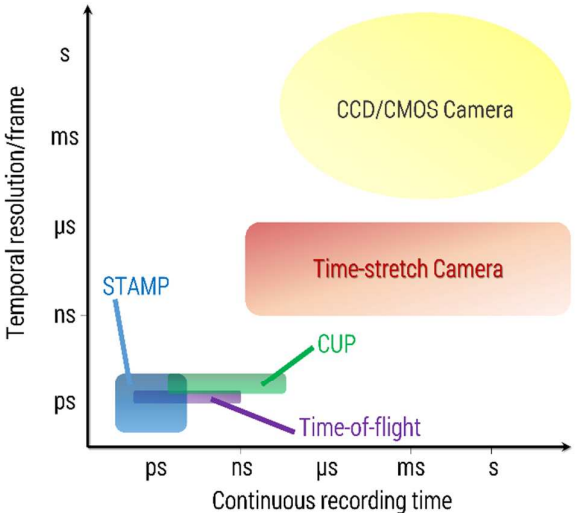

Fig. 1 Comparison of current ultrafast optical imaging techniques. Temporal resolution refers to the shutter speed or the frame time of the techniques. Time-stretch imaging provides a unique solution with a temporal resolution ranging from ns to μs and a continuous recoding time comparable to conventional CCD/CMOS cameras. Also note that other ultrafast imaging modalities achieve superior temporal resolution, down to ps or lower. However, they are operated in a streak mode, i.e. with limited continuous recording time. CUP: compressed ultrafast photography, STAMP: Sequentially timed all-optical mapping photography

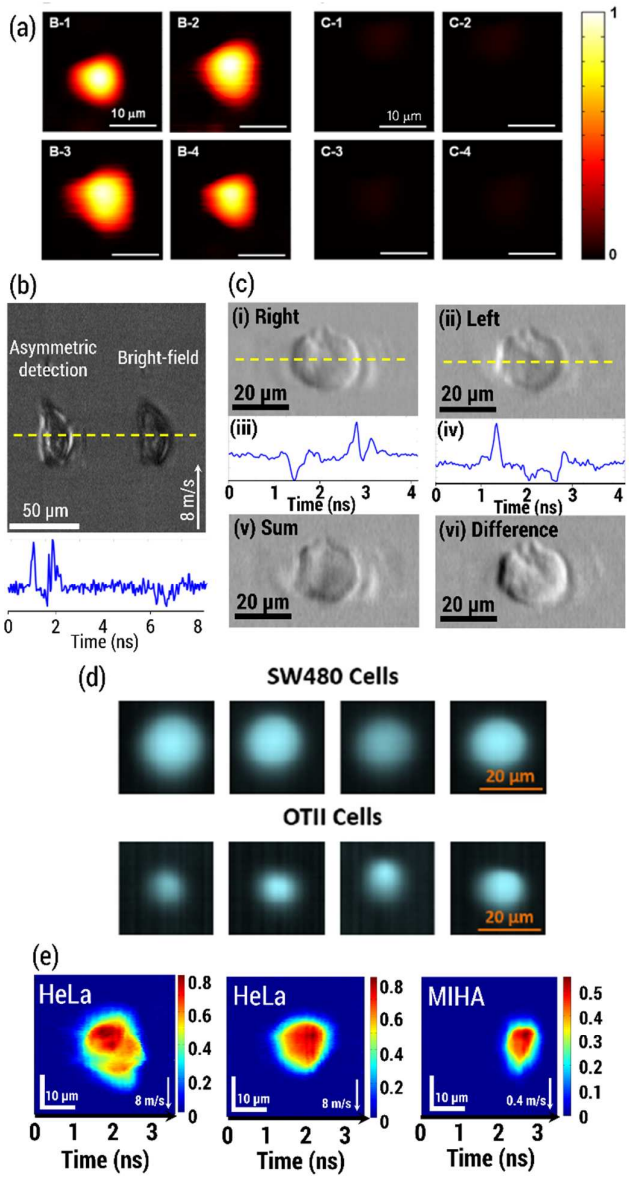

Fig. 4 (a) Nomarski time-stretch imaging (left four images of white blood cells) provides contrast enhancement. Compared to BF time-stretch imaging (right four images), the enhancement is > 15 times [26]. Scale bars represent 10 μm. (b) Improvement in image contrast of ATOM compared with BF time-stretch imaging. The bottom inset shows the line-scan of the yellow dashed line [29]. (c) ATOM Images of a hepatocyte with opposite shadows are shown in (i) and (ii). The line-scans of the yellow dashed line are shown in (iii) and (iv) to illustrate the opposite shadow effects. (v) and (vi) show the sum and difference images from images (i) and (ii) [29]. (d) Images of SW480 cells and OTII cells captured by quantitative phase-contrast time-stretch imaging operating at a line-scan rate of 36 MHz [106]. (e) Images of HeLa cells and MIHA cells flowing at 8 m/s and 0.4 m/s respectively, which are captured by quantitative phase-contrast time-stretch imaging operating at a line-scan rate of 26 MHz. White arrows indicate flow direction [30]. Color bars show the quantitative phase value in radians. It should be noted that a line-scan can be captured within 4 ns.

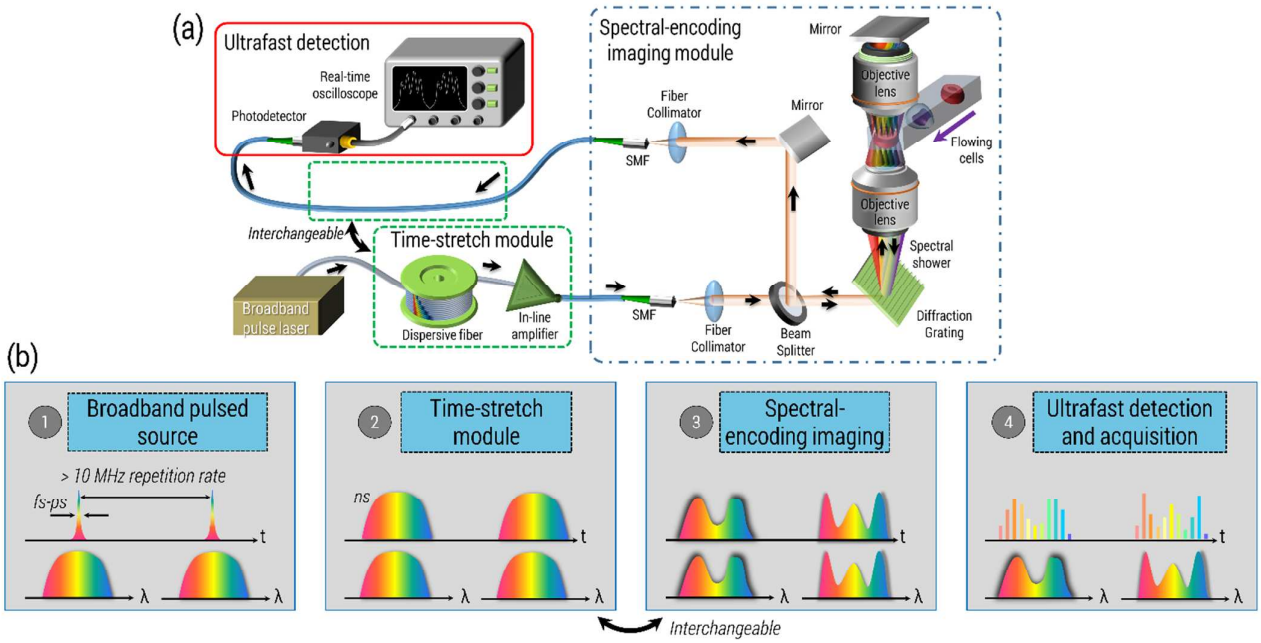

Fig. 2 (a) Schematics of optofluidic time-stretch imaging. (b) Ultrafast time-stretch imaging generally consists of four modules: a broadband pulsed laser source, a time-stretch module, a spectral-encoding imaging module and high-speed single-pixel detection. The time-stretch module and spectral-encoding imaging module is interchangeable with proper system design considerations. *t* and λ refer to time and optical wavelength.

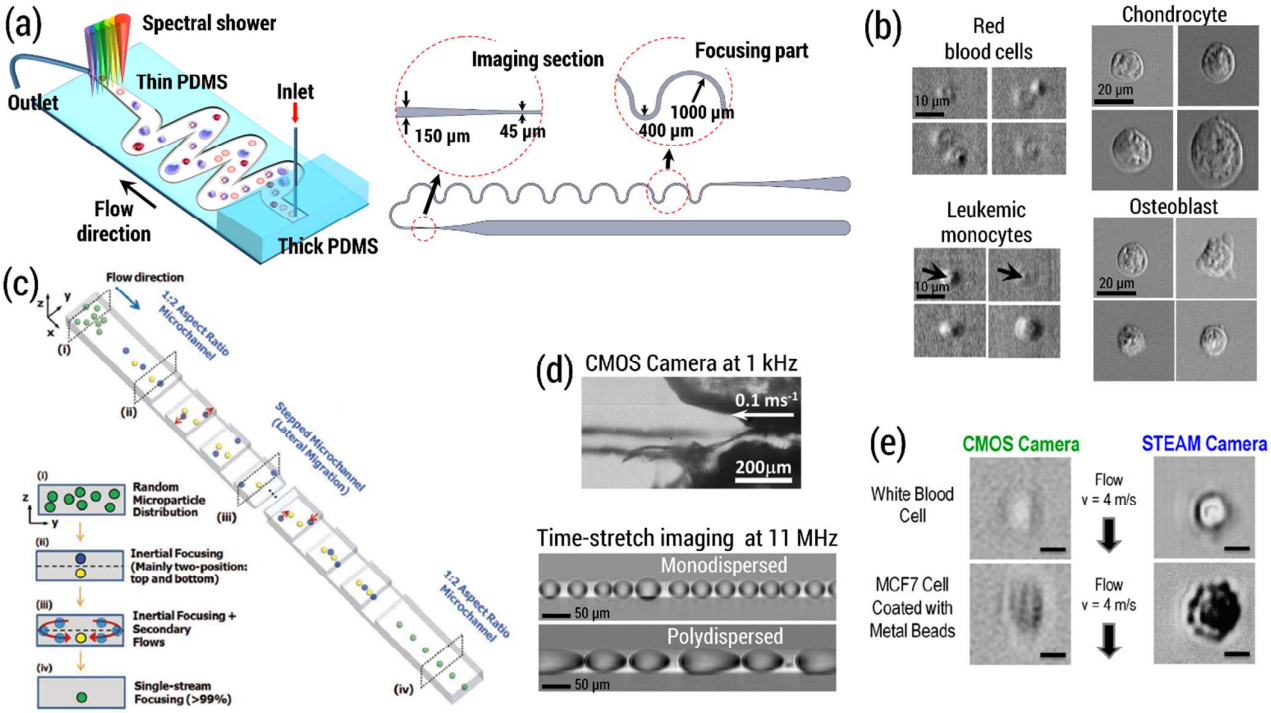

Fig. 3 (a) Microfluidic channel design used for time-stretch imaging that relies on inertial focusing scheme to constraint the position of flowing cells into a straight stream at the imaging region [27,29]. (b) Ultrafast time-stretch images of red blood cells and leukemic monocytes flowing up to 10 m/s, which are captured with a line-scan rate of 26 MHz [29]. Ultrafast time-stretch images of human osteoblast and chondrocyte flowing up to 3 m/s captured at 11 MHz. (c) Schematics of 3D, sheathless single-cell focusing channel [92]. (d) Ultrafast emulsion generation monitoring by time-stretch imaging at 11 MHz line-scan rate. Bottom image shows only a jet can be imaged by a CMOS camera at 1 kfps. (e) White blood cell and stained MCF7 cell images captured by CMOS and time-stretch cameras respectively. Again, only a blurred cell image can be captured by a CMOS camera [27]. Scale bars represent 10 μm.

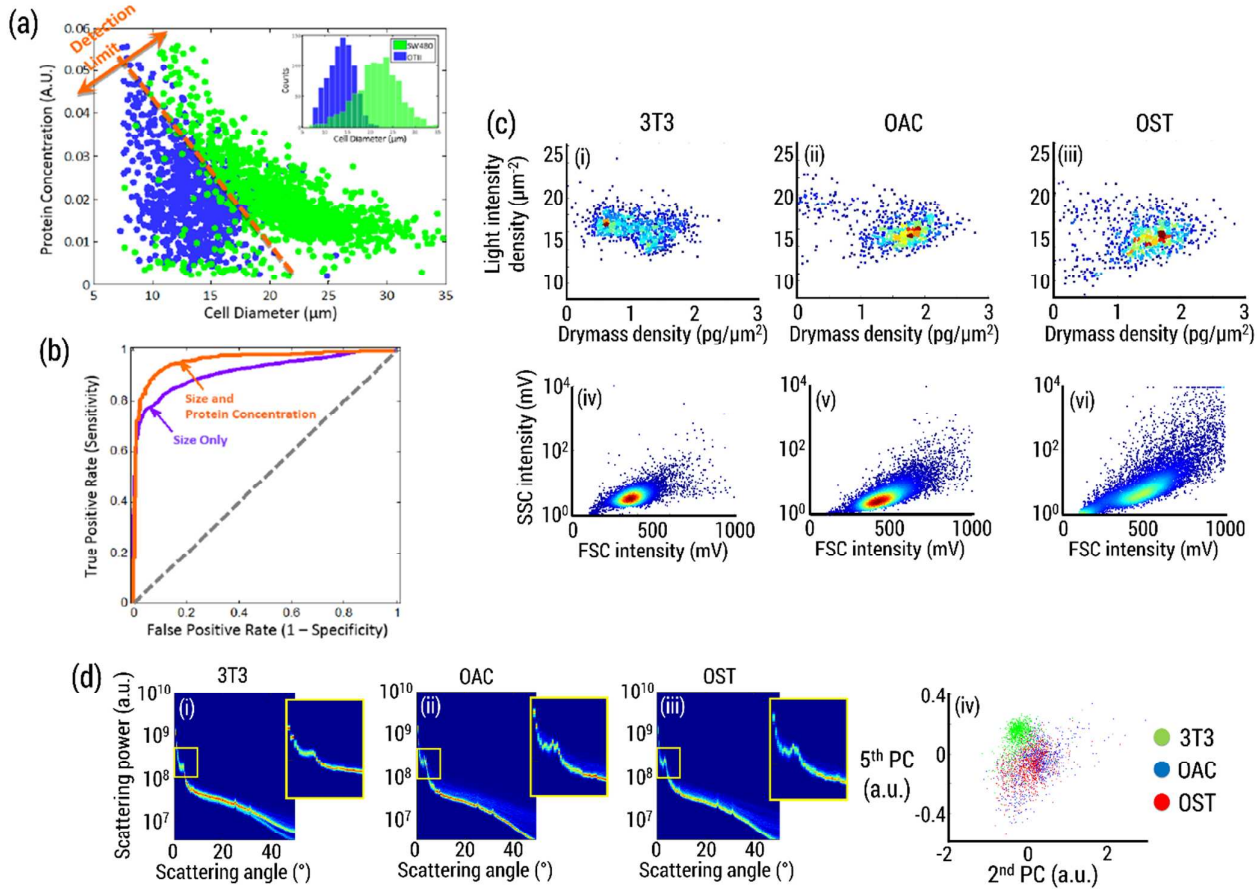

Fig. 5 (a) – (b) Comprehensive cellular analysis based on cell size, optical density and protein concentration in quantitative phase contrast time stretch imaging [106]. (c) (i) - (iii): scatter plots of light intensity density versus dry mass surface density for the three cell types, all extracted from quantitative phase contrast time-stretch imaging. (iv) - (vi): FSC versus SSC scatter plots of the three cell types obtained by conventional non-imaging flow cytometry. (d) Angular light scattering analysis of the three cell types. (i) – (iii) Insets show the zoom-in observation in the angle range of 0° – 4°, indicating a significant difference for these three cell types. (iv) Principal component analysis of the ALS curves of the three cell types, which shows 3T3 can be easily separated from the others. OAC: chondrocytes; OST: osteoblasts; 3T3: fibroblasts. FSC: forward scattering; SSC: side scattering. PC: principal component.